BULLETIN OF THE POLISH ACADEMY OF SCIENCES
TECHNICAL SCIENCES
Vol. 57, No. 4, 2009

Single phase full bridge inverter with coupled filter inductors and voltage doubler for PV module integrated converter system

Y. JIANG and J. PAN*

Department of Electrical Engineering, Shanghai Jiao Tong University, Shanghai 200240, P.R. China

Abstract. This paper presents a single phase full bridge inverter with coupled filter inductors and voltage doubler for PV module integrated converter (MIC) system. In DC/DC stage, full bridge circuit with high frequency sinusoidal pulse width modulation control is used, and high frequency transformer with voltage doubler rectifier circuit to increase conversional ratio is adopted. Finally, at the conversion end the rectified sinusoidal waveforms is generated. The coupled filter inductors, which are placed in voltage doubler, not only reduce circulating current, which increases efficiency but also make the rectified output sinusoidal waveforms of DC/DC stage as smooth voltage source. In DC/AC stage, the full bridge circuit with line frequency square wave control is adopted to reduce switching losses and control cost. To verify the presented analysis a 100 W prototype single phase 220 VAC 50 Hz inverter output has been constructed and the experimental results are given.

Key words: coupled filter inductors, circulating current, full bridge inverter, module integrated converter system, voltage doubler.

1. Introduction

Among a variety of the renewable energy sources, photovoltaic (PV) sources are predicted to become important contributors to electricity generation among all renewable energy candidates by 2040 [1]. Currently, there are three widely used PV systems: the centralized inverter system, the string inverter system and the module integrated converter (MIC) system [2–4]. Since the MIC system offers "plug and play" concept, it has become the trend for the future PV system development, however, challenges remain in terms of cost, reliability and stability [5–8]. As the MIC is most often fed from a single PV module, its typical power rating between 100 and 200 W are also quite common [9–17]. Among key system requirements there are: compactness, high reliability and low cost.

In the traditional MIC which is shown in Fig. 1, the power conversion process can be easily divided into two separate stages – DC/DC and DC/AC conversions [1]. In this arrangement, the DC/DC stage generates a constant dc link and sinusoidal pulse width modulation (SPWM) is used in the DC/AC inversion stage to produce AC waveforms that meet the prevailing harmonic standards. However, PWM control introduces additional switching losses and requires additional control circuitry. Gate drivers are more complex and control cost is higher. On the other hand, the main challenge for DC/DC stage is that it must have high conversion ratio to increase the low input voltage from PV panel.

In order to achieve high conversion ratio and increase efficiency in the DC/DC stage and also avoid the penalties associated with a PWM control in DC/AC stage, this paper proposes a single phase full bridge MIC with coupled filter inductors and voltage doubler shown in Fig. 2. The DC/DC stage generates rectified sinusoidal waveforms on the dc link. This makes it possible to reduce the output stage inverter to an unfolder using a simple line frequency square-wave control. The voltage doubler is adopted to increase conversion ratio, and the coupled filter inductors are placed in voltage doubler, The coupled inductors also reduce the circulating current which make the energy transfer back to source.

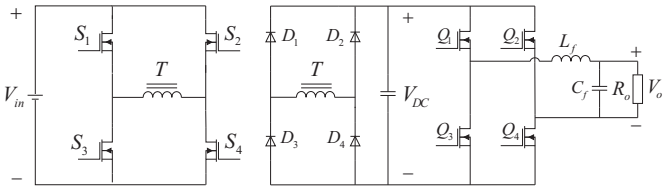

Fig. 1. Traditional commercial MIC

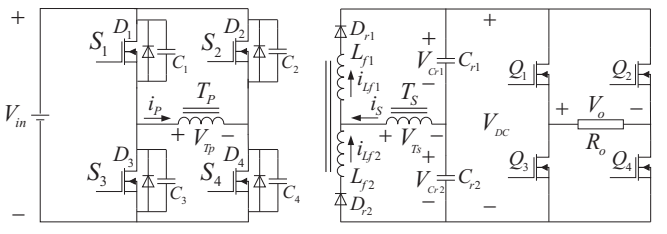

Fig. 2. Proposed MIC with coupled inductors and voltage doubler

The paper firstly studies DC/DC stage in detail. The operation and key features of the individual modes of the MIC

*e-mail: jmpan@sjtu.edu.cn

are discussed. The theoretical analyses are performed to explain the reducing of circulating current by coupled filter inductors. Also, the conversion ratio is analyzed. Secondly, the DC/AC stage with line frequency square-wave control is introduced. Finally, experimental results of a 100 W converter with 48-VDC input and 220 VAC 50 Hz output are provided at the end of the paper to confirm the theoretical analysis.

2. Operational principle

The proposed MIC system is shown in Fig. 2. Voltage-doubler and high frequency transformer are adopted to step up output voltage and coupled inductors L_{f1} and L_{f2} are adopted not only to be as filter inductors but also to reduce the circulating current. Several assumptions are made as follows:

1. Transformer includes primary side T_p and secondary side T_S, and their currents and voltages are i_p and i_S, V_{Tp} and V_{Ts} respectively, V_{Tp} /$V_{Ts} = i_S/i_P = n$, $L_{f1} = L_{f2}$, and their voltages areV_{Lf1} and V_{Lf2} respectively.
2. Switches S_{1-4} are ideal except for internal diodes ($D_1 = D_2 = D_3 = D_4$) and parasitic capacitors ($C_1 = C_2 = C_3 = C_4$) and switches Q_{1-4} are ideal.
3. The input voltage is V_{in}, R_o is load, V_o is valid value of AC output voltage.
4. Voltage doubler is ideal, rectifier capacitors C_{r1} and C_{r2} are identical and their voltages are V_{Cr1} and V_{Cr2} respectively, the output of the voltage doubler is V_{DC} and $V_{DC} = V_{Cr1} + V_{Cr2}$, V_{Cr1} and V_{Cr2} can be simplified as $V_{DC}/2$, D_{r1} and D_{r2} are rectifier diodes.

The operating waveforms of the proposed MIC system are shown in Fig.3. In Fig. 3a, the S_{1-4} in DC/DC stage are controlled by high frequency SPWM signals. The Q_{1-4} in DC/AC stage are controlled by line frequency square waveform signals. Finally, the rectified sinusoidal voltage V_{DC} is inverted into AC output voltage V_o. The high frequency operating waveforms of the proposed MIC are shown in Fig. 3b, and each switching period is subdivided into five modes which are shown in Fig. 4.

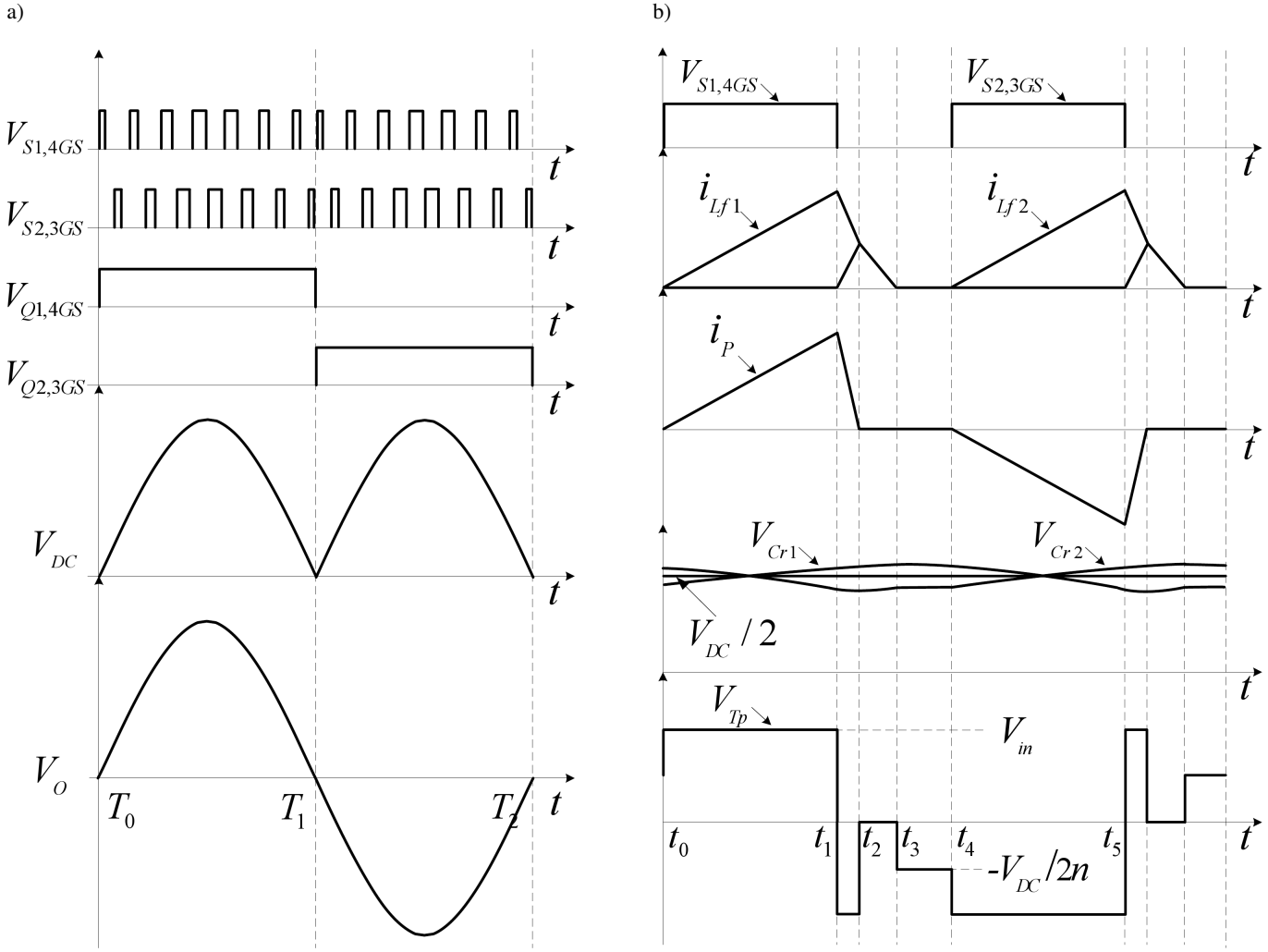

Fig. 3. Operating waveforms of the proposed MIC. (a) Operating waveforms of line frequency. (b) Operating waveforms of high

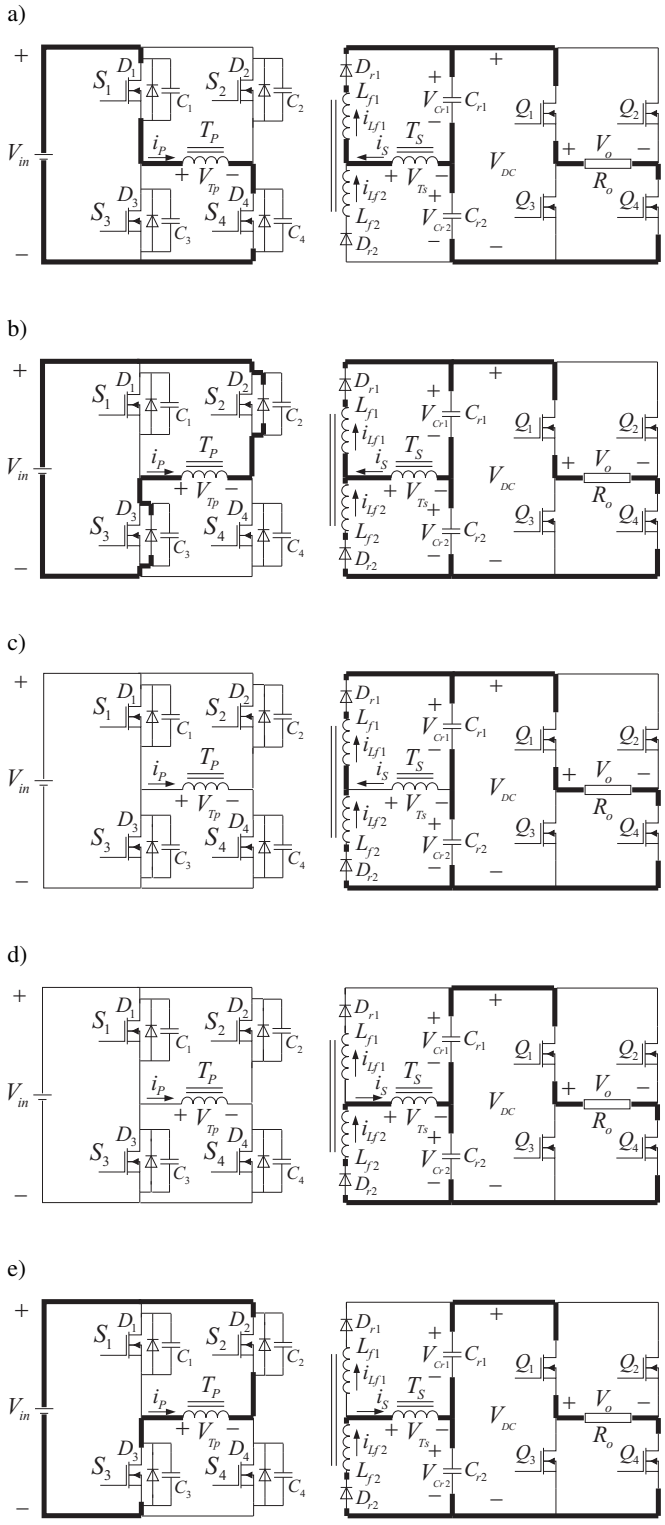

Fig. 4. Equivalent circuits of the proposed MIC for mode analysis. (a) Mode 1. (b) Mode 2. (c) Mode 3. (d) Mode 4. (e) Mode 5

1) Mode 1 ($t_0 \le t \le t_1$)**.** The gate signals of S_1 and S_4 are the same and they are turned on at the same time. The input voltage V_{in} is transferred to the primary side T_P, that is, $V_{Tp} = V_{in}$. D_{r2} is turned off, D_{r1} is turned on and C_{r1} is charged by $i_{Lf1}(t)$, that is, $i_{Lf2}(t) = 0$, $i_{Lf1}(t) = i_S(t)$ and $V_{Cr1} = V_{DC}/2$. $i_P(t) = ni_S(t)$ and $i_P(t)$ increases lineally from t_0. The voltage expression of coupled inductor L_{f1} can be represented as follows:

$$V_{Lf1} = nV_{in} - V_{DC}/2 = L_{f1}\frac{di_{Lf1}}{dt} + M\frac{di_{Lf2}}{dt}. \quad (1)$$

Since $i_{Lf2}(t) = 0$, and $i_P(t)$ can be represented as follows:

$$i_P(t) = ni_S(t) = ni_{Lf1}(t) = \\ = \frac{n}{L_{f1}}(nV_{in} - V_{DC}/2)(t - t_0). \quad (2)$$

where M is mutual inductance between L_{f1} and L_{f2}.

2) Mode 2 ($t_1 \le t \le t_2$). S_1 and S_4 are turned off at t_1. The current $i_P(t)$ decreases through D_2 and D_3, the energy is transferred back to source due to the circulating current, that is, $V_{Tp} = -nV_{in}$. D_{r1} and D_{r2} are turned on, $i_{Lf1}(t)$ decreases and $i_{Lf2}(t)$ increases, and $i_S(t) = i_{Lf1}(t) - i_{Lf2}(t)$. $V_{Cr1} = V_{Cr2} = V_{DC}/2$. The expression of coupled inductors L_{f1} and L_{f2}, $i_{Lf1}(t)$, $i_{Lf2}(t)$ and $i_P(t)$ can be represented as follows:

$$\begin{pmatrix} V_{Lf1} \\ V_{Lf2} \end{pmatrix} = \begin{pmatrix} -nV_{in} - V_{DC}/2 \\ nV_{in} - V_{DC}/2 \end{pmatrix} = \\ = \begin{pmatrix} L_{f1} & M \\ M & L_{f2} \end{pmatrix} \begin{pmatrix} \frac{di_{Lf1}}{dt} \\ \frac{di_{Lf2}}{dt} \end{pmatrix}, \quad (3)$$

$$i_{Lf1}(t) = i_{Lf1}(t_1) + \\ + \frac{L_{f2}(-nV_{in} - V_{DC}/2) - M(nV_{in} - V_{DC}/2)}{L_{f1}L_{f2} - M^2}(t - t_1), \quad (4)$$

$$i_{Lf2}(t) = \\ = \frac{L_{f1}(nV_{in} - V_{DC}/2) - M(-nV_{in} - V_{DC}/2)}{L_{f1}L_{f2} - M^2}(t - t_1), \quad (5)$$

$$i_P(t) = ni_S(t) = n(i_{Lf1}(t) - i_{Lf2}(t)) = \\ = ni_P(t_1) + n\left(\frac{(L_{f2} + M)(-nV_{in} - V_{DC}/2)}{L_{f1}L_{f2} - M^2} + \right. \\ \left. + \frac{(-L_{f1} - M)(nV_{in} - V_{DC}/2)}{L_{f1}L_{f2} - M^2}\right)(t - t_1). \quad (6)$$

3) Mode 3 ($t_2 \le t \le t_3$)**.** The current $i_P(t)$ decreases to zero. D_{r1} and D_{r2} are turned on, $i_{Lf1}(t) = i_{Lf2}(t)$, and $V_{Lf1} + V_{Lf2} = V_{Cr1} + V_{Cr2} = V_{DC}$. The voltage and current expressions of coupled inductors L_{f1} and L_{f2}, can be represented as follows:

$$V_{Lf1} + V_{Lf2} = L_{f1}\frac{di_{Lf1}}{dt} + M\frac{di_{Lf2}}{dt} + L_{f2}\frac{di_{Lf2}}{dt} + \\ + M\frac{di_{Lf1}}{dt} = V_{DC}, \tag{7}$$

$$i_{Lf1}(t) = i_{Lf2}(t) = \\ = i_{Lf1}(t_2) - \frac{V_{DC}}{L_{f1} + L_{f2} + 2M}(t - t_2). \tag{8}$$

4) Mode 4 ($t_3 \le t \le t_4$)**.** Currents $i_{Lf1}(t)$ and $i_{Lf2}(t)$ decrease to zero. Since C_{r1} is charged and C_{r2} is discharged in mode 1–3, V_{Cr1} is larger than V_{Cr2} in this mode and then D_{r2} is on and $i_{Lf2}(t)$ is not zero. However, $V_{Cr2-} - V_{Cr1}$ is much smaller and the inductance of T_P is much larger, $i_{Lf2}(t)$ is very small compared with modes 1–3 and can be seen as zero, thus V_{Ts} can be simplified as $-V_{Cr2}$, that is, $V_{Tp} = -V_{Cr2}/n = -V_{DC}/2n$.

5) Mode 5 ($t_3 \le t \le t_4$)**.** The primary current $i_P(t)$ flows through S_2 and S_3, another cycle is began, and the analyses are similar with modes 1–4.

3. Analysis of Coupled Inductors

In Fig. 5, i_p^- ($t_1 \le t \le t_2$) is circulating current which makes energy return back to source. In order to decrease the circulating current, the filter inductors L_{f1} and L_{f2} are coupled with each other is adopted. The dashed line ($t_1 < t < t_2'$) in Fig. 5 shows the currents $i_{Lf1}(t)$, $i_{Lf2}(t)$ and $i_P(t)$ when the L_{f1} and L_{f2} are discrete inductors and don't coupled with each other. In this case $i_{Lf1}(t)$, $i_{Lf2}(t)$ and $i_P(t)$ can be represented as follows:

$$i_{Lf1}(t) = i_{Lf1}(t_1) + \frac{-nV_{in} - V_{DC}/2}{L_{f1}}(t - t_1) \\ (t_1 < t < t_2'), \tag{9}$$

$$i_{Lf2}(t) = \frac{nV_{in} - V_{DC}/2}{L_{f2}}(t - t_1) \\ (t_1 < t < t_2'), \tag{10}$$

$$i_P(t) = ni_P(t_1) + \\ + n\frac{L_{f2}(-nV_{in} - V_{DC}/2) - L_{f1}(nV_{in} - V_{DC}/2)}{L_{f1}L_{f2}}(t - t_1) \\ (t_1 < t < t_2'). \tag{11}$$

Compared with (4), (5) and (6) where L_{f1} and L_{f2} are coupled with each other, since there is not mutual M in (9), (10) and (11), the slope of i_p^- in ($t_1 < t < t_2'$) is smoother than that in ($t_1 \le t \le t_2$), and then the energy transferred back to source by i_p^- is higher. Therefore, the coupled inductors is an effective method to reduce circulating current which is shown in ($t_1 \le t \le t_2$) in Fig. 5.

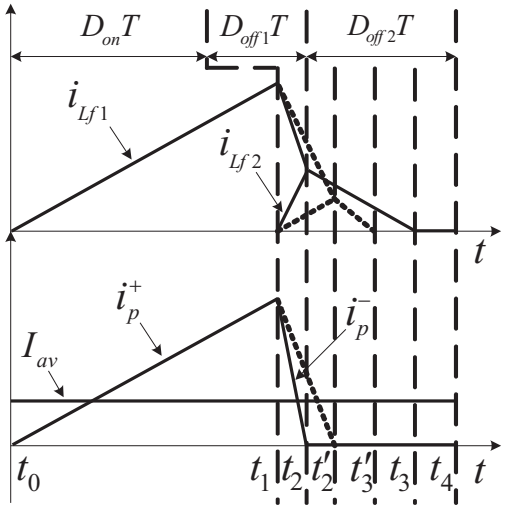

Fig. 5. Waveforms of the currents of coupled inductors and primary side of transformer

4. Analysis of conversion ratio

In order to analyze the conversion ratio M_{DC}, the waveform of primary current i_P shown in Fig. 5 is considered. For $T = t_4 - t_0$, i_p is described as i_p^+ ($t_0 \le t \le t_1$), i_p^- ($t_1 \le t \le t_2$), and I_{av} is the average value of i_p. M_{DC} is represented as follows:

$$M_{DC} = V_{DC\max}/V_{in}. \tag{12}$$

where $V_{DC\max}$ is the max value of V_{DC}.

I_{av} can be represented as follows:

$$I_{av}T = \int_{t_0}^{t_1} i_p^+ dt + \int_{t_1}^{t_2} i_p^- dt. \tag{13}$$

Based on Eqs. (2), (6), the i_p^+ and i_p^- can be represented as follows:

$$\begin{cases} i_p^+ = nB_{L1}(nV_{in} - V_{DC}/2)(t - t_0) \\ i_p^- = ni_p^+(t_1) - n(B_{L2}nV_{in} - B_{L3}V_{DC}/2)(t - t_1) \end{cases} \tag{14}$$

where

$$B_{L1} = \frac{1}{L_{f1}}, \\ B_{L2} = \frac{L_{f1} + L_{f2} + 2M}{L_{f1}L_{f2} - M^2}, \\ B_{L3} = \frac{L_{f1} - L_{f2}}{L_{f1}L_{f2} - M^2}. \tag{15}$$

I_{av} also can be represented as follows:

$$I_{av} = \frac{V_o^2}{V_{in}R_o} = \frac{\left(V_{DC\max}/\sqrt{2}\right)^2}{V_{in}R_o} = \frac{V_{DC\max}^2}{2V_{in}R_o}. \tag{16}$$

Based on (13)–(16), the conversion ratio M_{DC} can be got as follows:

$$M_{DC} = \frac{V_{DC\max}}{V_{in}} = \\ = \frac{1}{\frac{1}{4n}\frac{B_{13}}{B_{12}} + \frac{1}{2n}\sqrt{\frac{1}{4}\left(\frac{B_{13}}{B_{12}}\right)^2 + 4\frac{1}{R_o T B_{12}}}} \quad (17)$$

where

$$D_{on}T = t_1 - t_0,$$

$$D_{off1}T = t_2 - t_1,$$

$$B_{12} = B_{L1}D_{on}^2 + B_{L2}D_{off1}^2,$$

$$B_{13} = B_{L1}D_{on}^2 + B_{L3}D_{off1}^2.$$

From Eq. (17) it can be seen that conversional ratio M_{DC} depends on D_{on}, D_{off1}, L_{f1}, L_{f2}, M, R_o, cycle T and turns ratio n. It means that these parameters can be adjusted to satisfy the conversional ratio M_{DC} demanded.

5. Unfolder of DC/AC stage

As the input of the DC/AC stage is the rectified sinusoidal waveform, the square-wave control can be applied. In the DC/AC stage, the switches turn on and off with the line frequency.This avoids high switching losses caused by PWM control. The transfer function of the unfolder is

$$V_o = \begin{cases} V_{DC} = M_{DC}V_{in}, & Q_1 \text{ and } Q_4 \text{ on} \\ -V_{DC} = -M_{DC}V_{in}, & Q_2 \text{ and } Q_3 \text{ on} \end{cases}. \quad (18)$$

6. Experimental results

The parameters of proposed MIC system are shown as follows: transformer turns ratio $n = 4.5$, $L_{f1} = L_{f2} = 120$ μH, $M = 40$ μH, $C_{r1} = C_{r2} = 0.1$ μF, the max $D_{on} = 0.75$, the frequency in DC/DC stage is 50 kHz and in DC/AC stage is 50 Hz. Based on the designed parameters, a 100 W single phase MIC prototype with 48 VDC input and 220 VAC 50 Hz output is constructed. The Experimental operating waveforms of high frequency stage which $D_{on} = 0.5$ are shown in Fig. 6a–c. Figure 6a shows the primary side voltage of transformer V_{TP} and the primary side current i_P. It can be seen that when input power is imposed,i_P increases, and when input power is off, i_P decreases sharply due to the circulating current is reduced. Figure 6b shows the currents of i_{Lf1} and i_{Lf2}, and the waveforms agree with the coupling analysis to reduce the circulating current. Figure 6c shows the voltage V_{Cr1} and V_{Cr2} of voltage-doubler capacitors C_{r1} and C_{r2}. Duo to the interleaved voltage ripples and $V_{DC} = V_{Cr1} + V_{Cr2}$, and then the ripple of V_{DC} is reduced. The Experimental operating waveforms of line frequency are shown in Fig. 7a–b. Figure 7a shows the voltage V_{Cr1} and V_{Cr2} of line frequency, and each one is the rectified sinusoidal waveform. Since $V_{DC} = V_{Cr1} + V_{Cr2}$, it means the output of voltage-doubler V_{DC} is doubled, and then the conversional ratio is increased. Figure 7b shows the final AC output voltage V_o and current I_o.

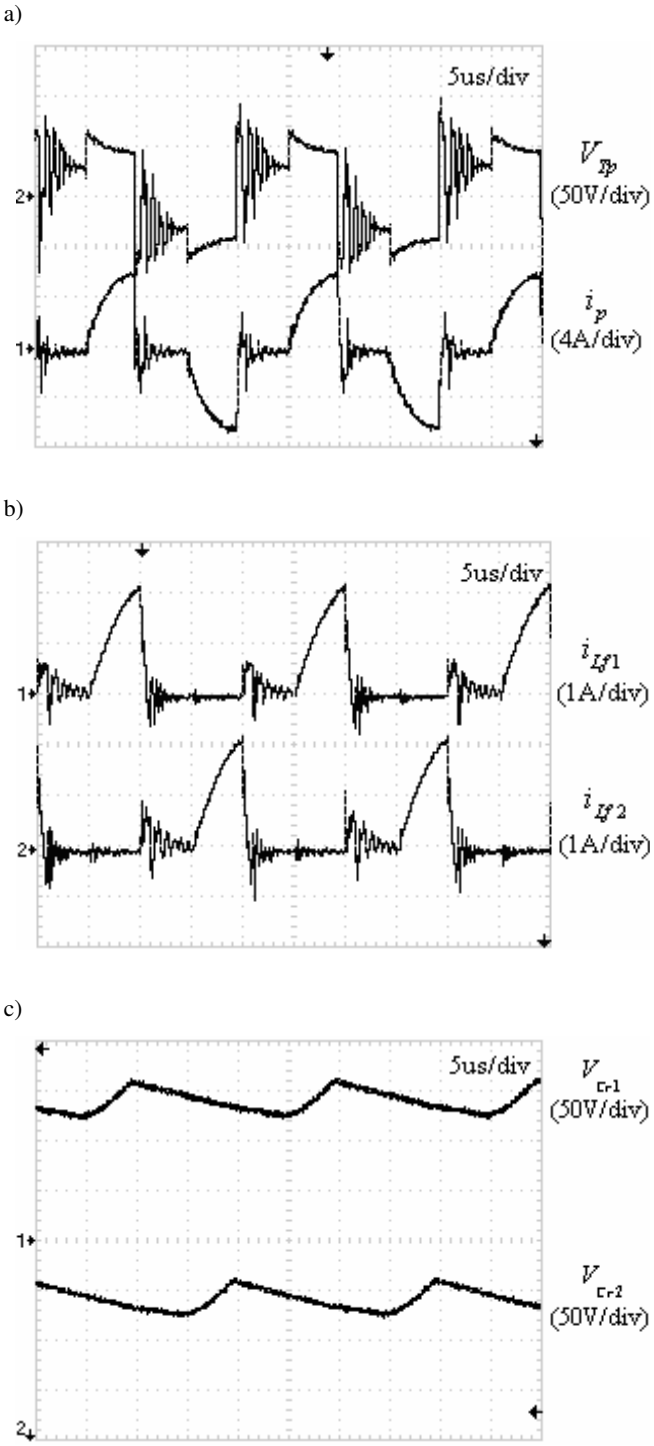

Fig. 6. Experimental operating waveforms of high frequency of proposed MIC. (a) Waveforms of V_{TP} and i_P. (b) Waveforms of i_{Lf1} and i_{Lf2}. (c) Waveforms of V_{Cr1} and V_{Cr2}

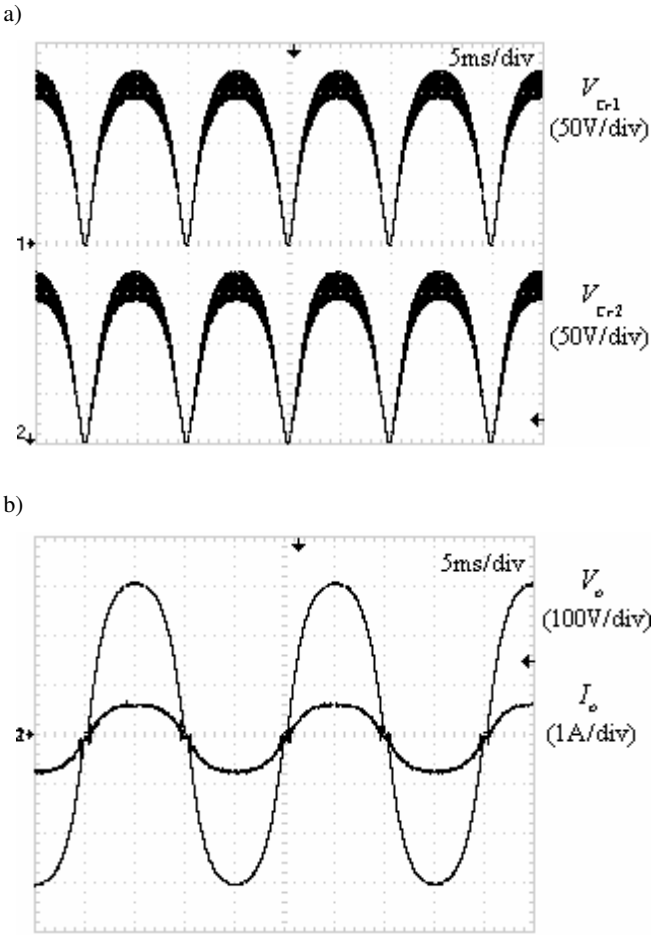

Fig. 7. Experimental operating waveforms of line frequency of proposed MIC. (a) Waveforms of V_{Cr1} and V_{Cr2}. (b) Waveforms of V_o and I_o

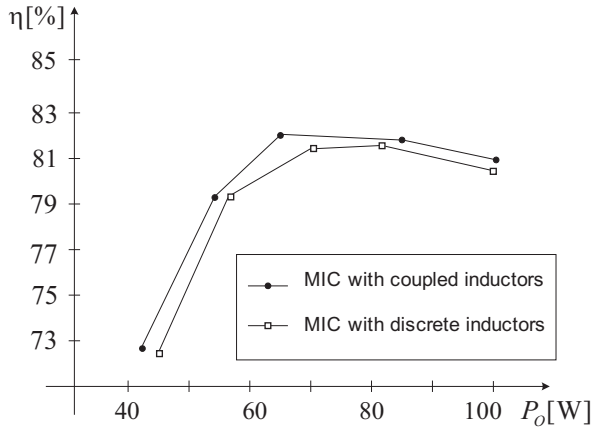

Fig. 8. Efficiency of the proposed MIC

The rectified sinusoidal voltage V_{DC} is inverted into sinusoidal voltage V_o, finally a resistive load is supplied and this is adjusted to give the rated power 100 W at 220 VAC. Due to the interleaved voltage ripples of V_{Cr1} and V_{Cr2}, the ripple of V_o is less than V_{Cr1} and V_{Cr2}. The efficiency comparison between coupled inductors and discrete inductors is shown in Fig. 8. It is noted that the proposed converter shows the higher efficiency over almost the entire load range because of the reducing of circulating current.

7. Conclusions

In this paper, a single phase full bridge inverter with coupled filter inductors and voltage doubler in PV module integrated system is proposed. The DC/DC stage operates in high frequency SPWM control to generate the rectified sinusoidal waveforms. The DC/AC stage operates in line frequency square-wave control to generate the sinusoidal waveforms and the switching losses and control circuitry is reduced. In DC/DC stage, the voltage doubler is adopted to increase conversional ratio and the coupled filter inductors are adopted to reduce the circulating current which make the energy transfer back to source. The experimental results of a 100 W prototype MIC have been presented to validate the theoretical analysis. The efficiency of the proposed converter is obtained about 81% at a rated condition.

REFERENCES

[1] European Renewable Energy Council, May, 2004 [Online]. Available: http://www.erec-renewables.org/documents/targets_2040/EREC_Scenario%202040.pdf, Renewable Energy Scenario to 2040 [Online]. Available.

[2] S.B. Kjær, J.K. Pedersen, and F. Blaabjerg, "Power inverter topologies for photovoltaic modules – a review," *Proc. IEEE IAS'02 Conf.* 1, 782–788 (2002).

[3] Y. Jiang, Z. Chen, J. Pan, X.I. Zhao, and P. Lee, "A novel phase-shift full-bridge converter with voltage-doubler and decoupling integrated magnetics in PV system", *Bull. Pol. Ac.: Tech.* 56 (3), 285–293 (2008).

[4] S. B. Kjær, J. K. Pedersen, and F. Blaabjerg, "A review of single-phase grid-connected inverters for photovoltaic modules," *IEEE Trans. Ind. Appl.* 41 (5), 1292–1306 (2005).

[5] Quan Li, and Peter Wolfs, "A review of single phase photovoltaic module integrated converter topologies with three different DC link configurations", *IEEE Trans. Power Electron.* 23 (3), 1320–1332 (2008).

[6] M. Meinhardt and G. Cramer, "Past, present and future of grid connected photovoltaic- and hybrid-power-systems", *Proc. IEEE-PES Summer Meeting* 2, 1283–1288 (2000).

[7] Jong-Pil Lee, Byung-Duk Min, Tae-Jin Kim, Dong-Wook Yoo, and Ji-Yoon Yoo, "A novel topology for photovoltaic DC/DC full-bridge converter with flat efficiency under wide PV module voltage and load range", *IEEE Trans. Ind. Electron.* 55 (7), 2602–2609 (2008).

[8] S.B. Kjær and F. Blaabjerg, "Design optimization of a single phase inverter for photovoltaic applications," *Proc. IEEE PESC'03 Conf.* 1, 1183–1190 (2003).

[9] S.B. Kjær and F. Blaabjerg, "A novel single-stage inverter for the AC-module with reduced low-frequency ripple penetration", *Proc. Eur. Conf. Power Electron. Appl.* 1, 1–10 (2003).

[10] N. Kasa, T. Iida, and A.K.S. Bhat, "Zero-voltage transition flyback inverter for small scale photovoltaic power system", *Proc. IEEE PESC'05 Conf.* 1, 2098–2103 (2005).

[11] N. Kasa, T. Iida, and L. Chen, "Flyback inverter controlled by sensorless current MPPT for photovoltaic power system", *IEEE Trans. Ind. Electron.* 52 (4), 1145–1152 (2005).

[12] M. Meinhardt, T. O'Donnell, H. Schneider, J. Flannery, C.Ó. Mathuna, P. Zacharias, and T. Krieger, "Miniaturised low profile module integrated converter for photovoltaic applications with integrated magnetic components", *Proc. IEEE APEC'99 Conf.* 1, 305–311 (1999).

[13] Q. Li and P. Wolfs, "A current fed two-inductor boost converter with an integrated magnetic structure and passive lossless snubbers for photovoltaic module integrated converter applications", *IEEE Trans. Power Electron.* 22 (1), 309–321 (2007).

[14] E. Roman, R. Alonso, P. Ibanez, S. Elorduizapatarietxe, and D. Goitia, "Intelligent PV module for grid-connected PV systems", *IEEE Trans. Ind. Electron.* 53 (4), 1066–1073 (2006).

[15] Y. Xue, L. Chang, S.B. Kjaer, J. Bordonau, and T. Shimizu, "Topologies of single-phase inverters for small distributed power generators: an overview", *IEEE Trans. Power Electron.* 19 (5), 1305–1314 (2004).

[16] Q. Li and P. Wolfs, "The power loss optimisation of a current fed ZVS two-inductor boost converter with a resonant transition gate drive", *IEEE Trans. Power Electron.* 21 (5), 1253–1263 (2006).

[17] Z.Chen, X. Zhang, and J.Pan, "An integrated inverter for a single-phase single-stage grid-connected PV system based on Z-source", *Bull. Pol. Ac.: Tech.* 55 (3), 263–272 (2007).